U.S. DEPARTMENT OF COMMERCE
NATIONAL OCEANIC AND ATMOSPHERIC ADMINISTRATION
OCEAN PRODUCTS CENTER

TECHNICAL NOTE

ESTIMATING SURFACE CURRENTS IN THE SLOPE WATER REGION BETWEEN 37 AND 41°N USING SATELLITE FEATURE TRACKING

LAURENCE C. BREAKER, LAWRENCE D. BURROUGHS, THOMAS B. STANLEY
AND WALTON B. CAMPBELL

NATIONAL METEOROLOGICAL CENTER
WASHINGTON, D. C.
FEBRUARY 1992

OPC Contribution No. 48

OPC CONTRIBUTIONS

No. 1. Burroughs, L. D., 1986: Development of Forecast Guidance for Santa Ana Conditions. National Weather Digest, Vol. 12 No. 1, 8pp.

No. 2. Richardson, W. S., D. J. Schwab, Y. Y. Chao, and D. M. Wright, 1986: Lake Erie Wave Height Forecasts Generated by Empirical and Dynamical Methods -- Comparison and Verification. Technical Note, 23pp.

No. 3. Auer, S. J., 1986: Determination of Errors in LFM Forecasts Surface Lows Over the Northwest Atlantic Ocean. Technical Note/NMC Office Note No. 313, 17pp.

No. 4. Rao, D. B., S. D. Steenrod, and B. V. Sanchez, 1987: A Method of Calculating the Total Flow from A Given Sea Surface Topography. NASA Technical Memorandum 87799., 19pp.

No. 5. Feit, D. M., 1986: Compendium of Marine Meteorological and Oceanographic Products of the Ocean Products Center. NOAA Technical Memorandum NWS NMC 68, 93pp.

No. 6. Auer, S. J., 1986: A Comparison of the LFM, Spectral, and ECMWF Numerical Model Forecasts of Deepening Oceanic Cyclones During One Cool Season. Technical Note/NMC Office Note No. 312, 20pp.

No. 7. Burroughs, L. D., 1987: Development of Open Fog Forecasting Regions. Technical Note/NMC Office Note. No. 323., 36pp.

No. 8. Yu, T. W., 1987: A Technique of Deducing Wind Direction from Satellite Measurements of Wind Speed. Monthly Weather Review, 115, 1929-1939.

No. 9. Auer, S. J., 1987: Five-Year Climatological Survey of the Gulf Stream System and Its Associated Rings. Journal of Geophysical Research, 92, 11,709-11,726.

No. 10. Chao, Y. Y., 1987: Forecasting Wave Conditions Affected by Currents and Bottom Topography. Technical Note, 11pp.

No. 11. Esteva, D. C., 1987: The Editing and Averaging of Altimeter Wave and Wind Data. Technical Note, 4pp.

No. 12. Feit, D. M., 1987: Forecasting Superstructure Icing for Alaskan Waters. National Weather Digest, 12, 5-10.

No. 13. Sanchez, B. V., D. B. Rao, S. D. Steenrod, 1987: Tidal Estimation in the Atlantic and Indian Oceans. Marine Geodesy, 10, 309-350.

No. 14. Gemmill, W.H., T.W. Yu, and D.M. Feit 1988: Performance of Techniques Used to Derive Ocean Surface Winds. Technical Note/NMC Office Note No. 330, 34pp.

No. 15. Gemmill, W.H., T.W. Yu, and D.M. Feit 1987: Performance Statistics of Techniques Used to Determine Ocean Surface Winds. Conference Preprint, Workshop Proceedings AES/CMOS 2nd Workshop of Operational Meteorology, Halifax, Nova Scotia., 234-243.

No. 16. Yu, T.W., 1988: A Method for Determining Equivalent Depths of the Atmospheric Boundary Layer Over the Oceans. Journal of Geophysical Research. 93, 3655-3661.

No. 17. Yu, T.W., 1987: Analysis of the Atmospheric Mixed Layer Heights Over the Oceans. Conference Preprint, Workshop Proceedings AES/CMOS 2nd Workshop of Operational Meteorology, Halifax, Nova Scotia, 2, 425-432.

No. 18. Feit, D. M., 1987: An Operational Forecast System for Superstructure Icing. Proceedings Fourth Conference Meteorology and Oceanography of the Coastal Zone. 4pp.

No. 19. Esteva, D.C., 1988: Evaluation of Priliminary Experiments Assimilating Seasat Significant Wave Height into a Spectral Wave Model. Journal of Geophysical Research. 93, 14,099-14,105

No. 20. Chao, Y.Y., 1988: Evaluation of Wave Forecast for the Gulf of Mexico. Proceedings Fourth Conference Meteorology and Oceanography of the Coastal Zone, 42-49

No. 21. Breaker, L.C., 1989: El Nino and Related Variability in Sea-Surface Temperature Along the Central California Coast. PACLIM Monograph of Climate Variability of the Eastern North Pacific and Western North America, Geophysical Monograph 55, AGU, 133-140.

No. 22. Yu, T.W., D.C. Esteva, and R.L. Teboulle, 1991: A Feasibility Study on Operational Use of Geosat Wind and Wave Data at the National Meteorological Center. Technical Note/NMC Office Note No. 380, 28pp.

No. 23. Burroughs, L. D., 1989: Open Ocean Fog and Visibility Forecasting Guidance System. Technical Note/NMC Office Note No. 348, 18pp.

No. 24. Gerald, V. M., 1987: Synoptic Surface Marine Data Monitoring. Technical Note/NMC Office Note No. 335, 10pp.

No. 25. Breaker, L. C., 1989: Estimating and Removing Sensor Induced Correlation form AVHRR Data. Journal of Geophysical Reseach, 95, 9701-9711.

No. 26. Chen, H. S., 1990: Infinite Elements for Water Wave Radiation and Scattering. International Journal for Numerical Methods in Fluids, 11, 555-569.

No. 27. Gemmill, W.H., T.W. Yu, and D.M. Feit, 1988: A Statistical Comparison of Methods for Determining Ocean Surface Winds. Journal of Weather and Forecasting. 3, 153-160.

No. 28. Rao. D. B., 1989: A Review of the Program of the Ocean Products Center. Weather and Forecasting. 4, 427-443.

1. INTRODUCTION

In support of NOAA's COASTWATCH[1] requirements, an effort is underway to develop a capability to estimate surface currents in coastal areas around the United States using sequential Advanced Very High Resolution Radiometer infrared (AVHRR IR) satellite imagery from NOAA's Polar-Orbiting satellites. The technique is referred to as "feature tracking", and as the name implies, the locations of selected ocean features (in this case thermal features) are tracked from one image to the next from co-registered image pairs. Displacements can be calculated by locating features in successive images and calculating the corresponding separation distance. Once the displacements have been determined, it is straightforward to calculate the velocities based on the time interval between the images.

An area in the Slope Water (SW) region off the U.S. east coast between 37°N and 41°N was selected for this study (Fig.1). This region is an area of interest to COASTWATCH since it corresponds to one of the high-resolution coastal sectors in the Northeast COASTWATCH region. Also, AVHRR satellite data are readily available for this area. In addition, this area avoids the Gulf Stream further offshore where trackable thermal features often do not exist. Finally, we have briefly examined wind forcing and its possible contribution to the surface circulation in this area although this was not our primary goal.

---

[1]A project of NOAA's Coastal Ocean Program.

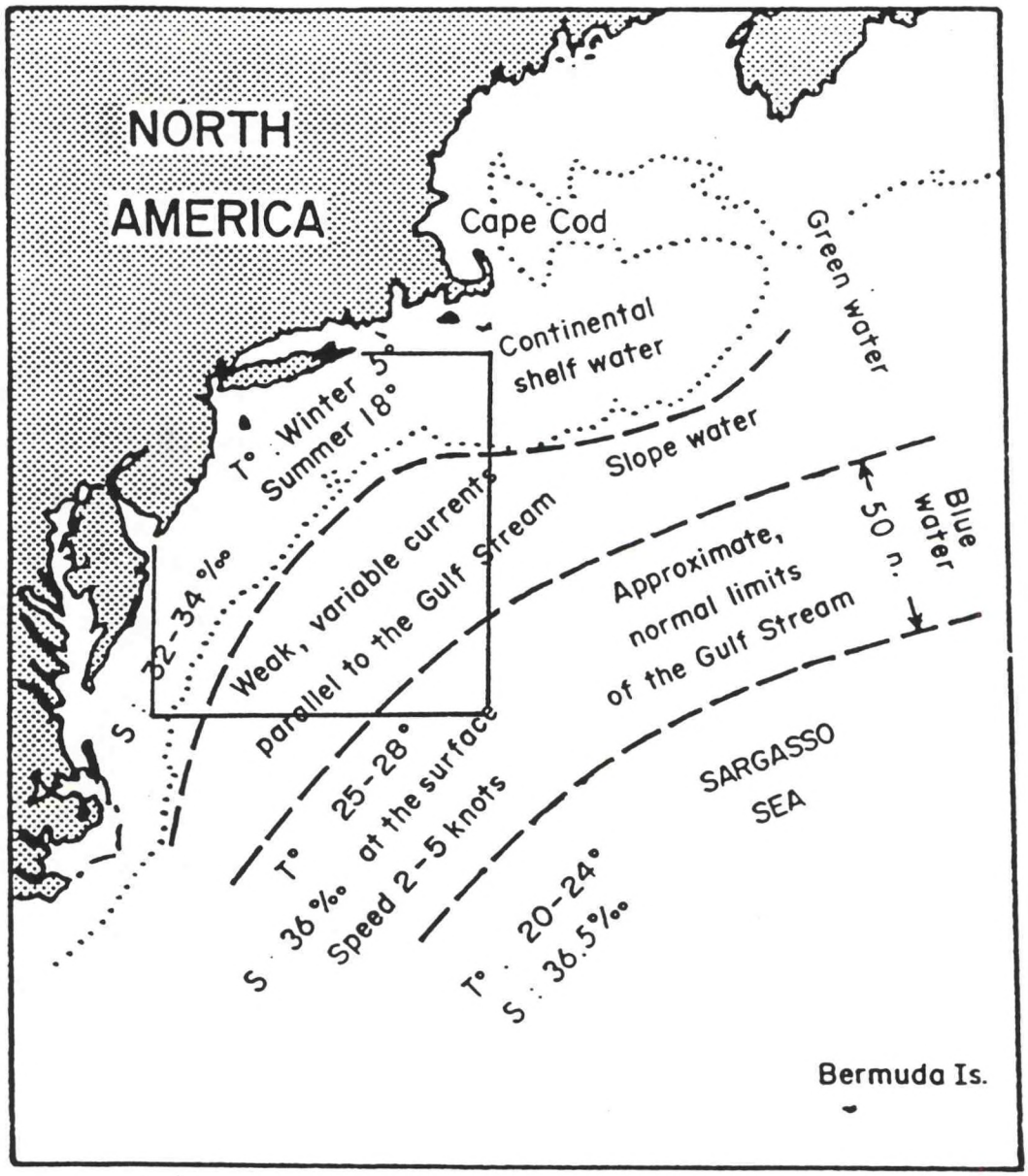

Figure 1. Distribution of waters off the east coast of the United States (from Tchernia, 1980). The study area is shown and extends from 37-41°N and from 70-74°W (rectangle outlined with solid lines).

2. FEATURE TRACKING

The technique of feature tracking is often referred to as change detection analysis in remote sensing and has a long history associated with military reconnaissance (e.g., Rosenfeld, 1961). The technique has been used by meteorologists to estimate low level winds by tracking cloud motions (e.g., Sadler, 1962; Sadler, 1963; Leese et al., 1971) and to determine sea ice motion (Ninnis et al., 1986). In meteorology, the levels at which the tracked motions occur are often not known precisely. But, in satellite oceanography when sea surface temperature (SST) is used as a tracer, the level corresponds very closely to the ocean surface.[2] This technique has only been feasible in satellite oceanography for the past 10 years or so due to significant improvements made in the earth location of satellite image data. Because of the relatively long time scales and small space scales associated with typical ocean features and their motion, accuracy requirements for earth location in oceanography are far more stringent than they are in meteorology.

A number of assumptions, limitations and sources of error arise with respect to ocean feature tracking in using SST as a tracer. First, for AVHRR IR data it is assumed that temperature acts as a conservative passive tracer (Abbott and Chelton, 1991).

---

[2]If ocean color is used as a tracer, the actual level is more difficult to specify since the outgoing radiance from the ocean surface includes contributions from levels below the surface down to several tens of meters.

The technique attempts to capture the advective motion associated with submesoscale features (Njoku et al., 1985). When SST signatures of wave motion are present, it may be difficult to distinguish between the sought-after advective motion, and wave-related phase velocities. Also, in satellite feature tracking, it is assumed that the motion between images is rectilinear (usually there is no alternative), an assumption whose validity we will later examine.

Several limitations exist with respect to satellite feature tracking. First, cloud cover often obscures the ocean surface, and second, unique, identifiable features must persist over the period between two successive images. Regions such as the core of the Gulf Stream, for example, are not usually amenable to feature tracking since this area often lacks sharp and distinct thermal gradients which can be tracked. Finally, it must be understood that the feature tracking technique only attempts to capture the instantaneous flow at specific times and locations (without regard to the underlying processes that contribute to this flow) and as a result should not be directly taken as a measure of the mean flow.

Several potential sources of error exist with respect to feature tracking. Errors in the earth location of image pixels, for example, directly affect the velocity estimates; such errors, if they exist, must be determined and taken into account.[3] Also, co-registration errors of ± 1 pixel produce velocity errors of

---

[3]In practice, it may only be necessary to distinguish between ascending and descending orbits since errors in navigation may be self-cancelling for a given orbit orientation.

± 2.5 cm/sec for image separations of 12 hours (Wahl and Simpson, 1990). Another consideration in estimating surface velocities relates to the optimum time interval between images. At one extreme, if the time interval between images is too short (say less than 6 hours), then the displacements may be so small as to be comparable in magnitude to other errors such as earth location. At the other extreme, if the time interval between images is too long, it becomes difficult to unambiguously identify the individual features that are being tracked and the assumption of rectilinear motion between the images becomes questionable. Svejkovsky (1988) found that time intervals of 12 to 24 hours were optimal. Conversely, Tokmakian et al. (1990) recommended that time intervals as short as possible between images be employed. Our study likewise addresses this question.

Based on kinematical considerations, the displacements of selected features obtained from feature tracking are best described by a Lagrangian representation. This representation provides a displacement history or trajectory of the motion experienced by fluid particles. Thus, if the initial position of a selected water particle at time t_o is given as x_o, y_o, then the Lagrangian representation expresses the position x, y, of that particle at time t as

$$x = x\ (x_o,\ y_o,\ t-t_o)$$

and

$$y = y\ (x_o,\ y_o,\ t-t_o)$$

To determine the corresponding velocities, u and v,

$$u = \frac{\partial x(x_o, y_o, t)}{\partial t}$$

and

$$v = \frac{\partial y(x_o, y_o, t)}{\partial t}$$

To the extent that the apparent water movement is advective, these equations describe the motion revealed through feature tracking.

In the following analyses, we use AVHRR IR satellite imagery from Channel 4 (10.3 to 11.3 microns) with a spatial resolution of 1.1 km and a thermal resolution of approximately 0.2°C. Three AVHRR IR images were used in the analysis and were acquired at 0733Z and 1859Z on June 24th, and at 1847Z on June 25th; thus the time separations are 11.43 hours between the first and second images, 23.80 hours between the second and third images, and 35.23 hours between the first and third images. By selecting a sequence of three cloud-free images which were contiguous in time, we were able to examine the continuity of the flow and the assumption of rectilinear motion. The area of the study extends from 37°N to 41°N and from 70°W to 74°W (the area outlined in Fig. 1). The oceanographic regime of primary interest is the Slope Water region located between the continental shelf and the Gulf Stream. We have included within our analysis region the area overlying, and slightly shoreward of, the continental shelf break.

At the present time, feature tracking is conducted interactively; i.e, an analyst decides which features are to be tracked. Automated/objective procedures for determining the surface flow field such as the maximum cross-correlation technique (Emery et al., 1986) may be more desirable and will be developed in the future. We believe, however, that it is important for an analyst to be involved at least initially in applying this technique to new areas where the general characteristics of the flow field may be unfamiliar. Automated procedures may also miss fine-scale structure in the flow field depending on the length scales employed, plus they may be insensitive to rotational and deformational motions (Kamachi, 1989). The maximum cross-correlation technique is additionally time consuming computationally (Tokmakian et al., 1990).

The present analysis system consists of an IBM-compatible PC workstation, 80 megabytes of storage and a Revolution 512 x 32 graphics coprocessor. The display provides 512 x 484 pixel resolution. Because this system only allows one image to be examined at a time, feature tracking in this case was tedious and lengthy. By determining the locations of the selected features in two successive images, the feature displacements were found by calculating the great circle distances between the locations. Dividing these displacements by the time separation between images produced the desired velocities.

3. ENVIRONMENTAL CONDITIONS

a. Meteorological

At the beginning of the study period (00 UTC on 24 June), an area of low pressure centered at 36°N, 71°W and moving to the Northeast, was followed by clearing skies with northerly winds of about 8 m/sec (Fig. 2). By 06 UTC on the 25th, the low had moved further to the Northeast with sea level pressure in the study area gradually increasing (Fig. 3). Later on the 25th, the area was dominated by high pressure providing clear skies and light winds (~3 m/sec) from the east southeast (ESE).

b. Oceanographic

The Slope Water region spans the area between the continental shelf break and the Gulf Stream. The circulation in this region is dominated by the southwestward flow of relatively fresh water from the Labrador Current. Generally, the surface currents in this region are weak and variable but tend to flow more-or-less parallel to the Gulf Stream but in the opposite direction. The flow is frequently disturbed by anticyclonic warm-core eddies often with waters entrained from the Gulf Stream and the Sargasso Sea. These eddies may be as large as 200-300km in diameter. Their movement, which is generally to the SW (~ 3-8 cm/sec), is constrained by the locations of the continental margin and the Gulf Stream (Richardson, 1983). Another prominent feature in the Slope Water region is the shelf/slope front which is located along the outer

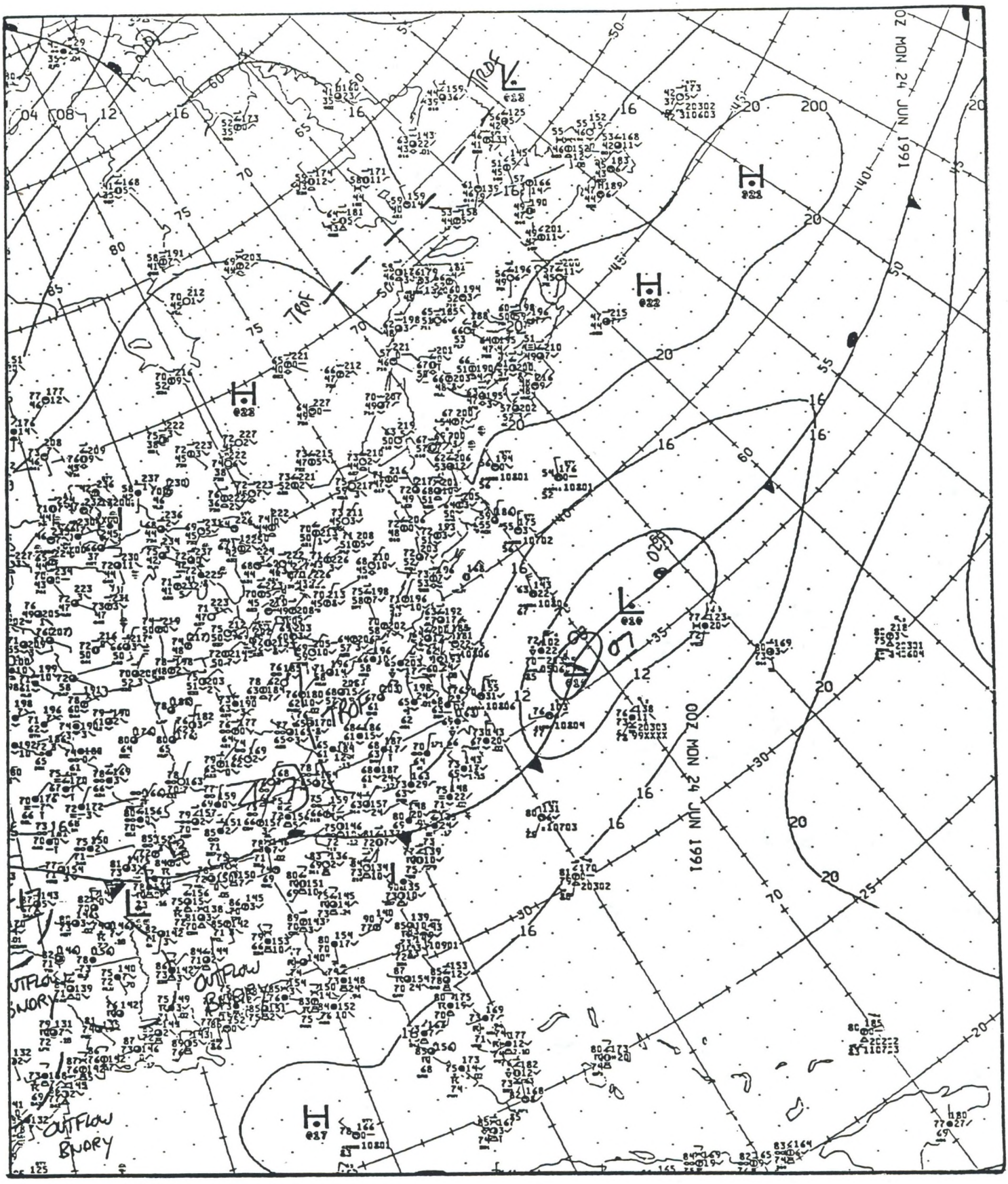

Figure 2. NMC surface analysis for 24 June 1991 at 0000 UTC.

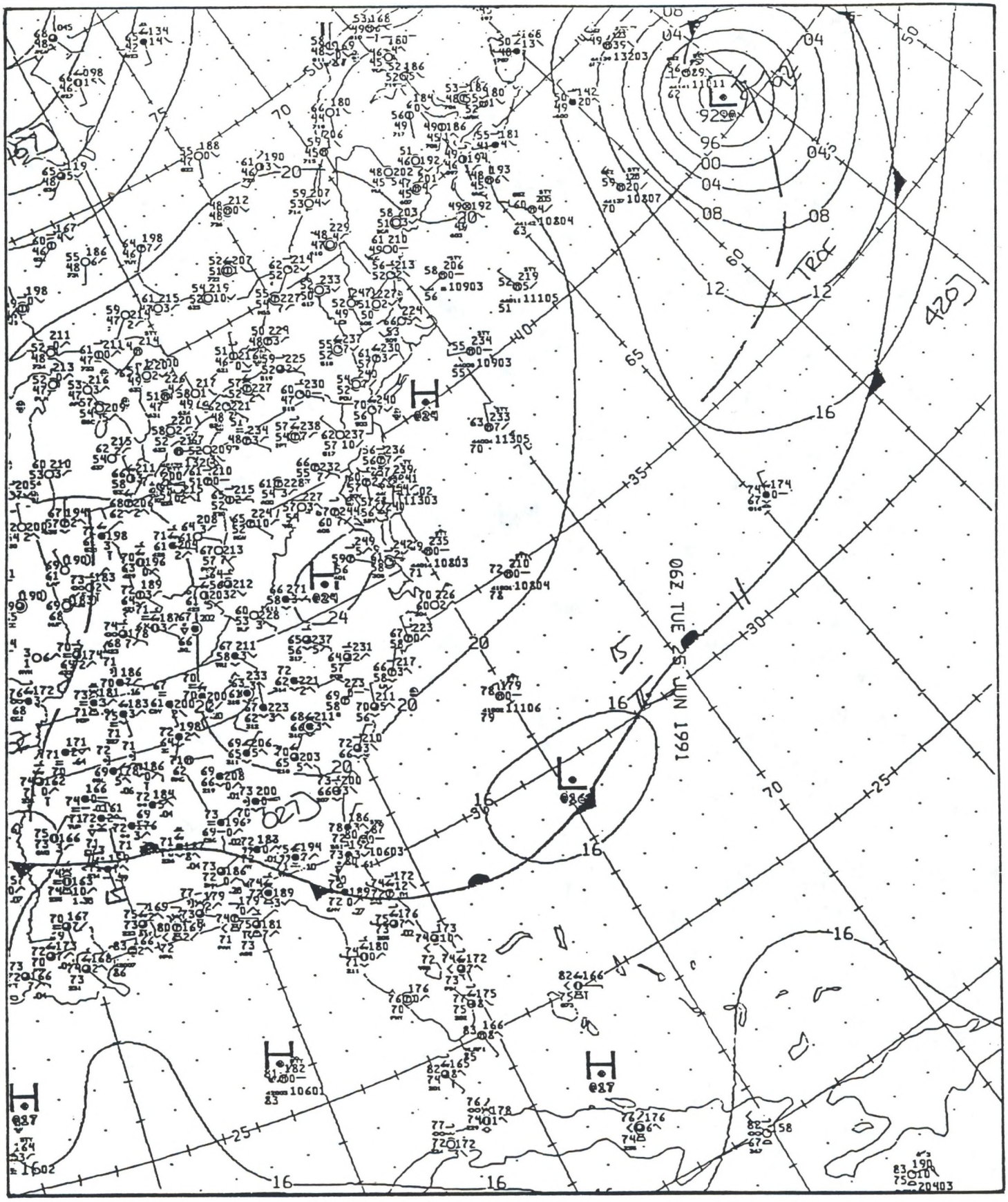

Figure 3. NMC surface analysis for 25 June 1991 at 0600 UTC.

continental shelf. This front typically overlies the continental shelf break (Mooers et al., 1978). It forms the transition between shelf waters near the coast and the slope waters further offshore. Although this frontal region is usually most intense during winter, it exists throughout the year. Both tidal and inertial oscillations contribute to variability along this front (Beardsley and Flagg, 1975).

Actual conditions encountered during the study period can be inferred from the satellite imagery shown in Figs. 4-6. These images clearly show the shelf/slope front and an eddy centered at 39.5N, 71.3W. Finally, just north of the Gulf Stream there is a major intrusion of warm Gulf Stream water.

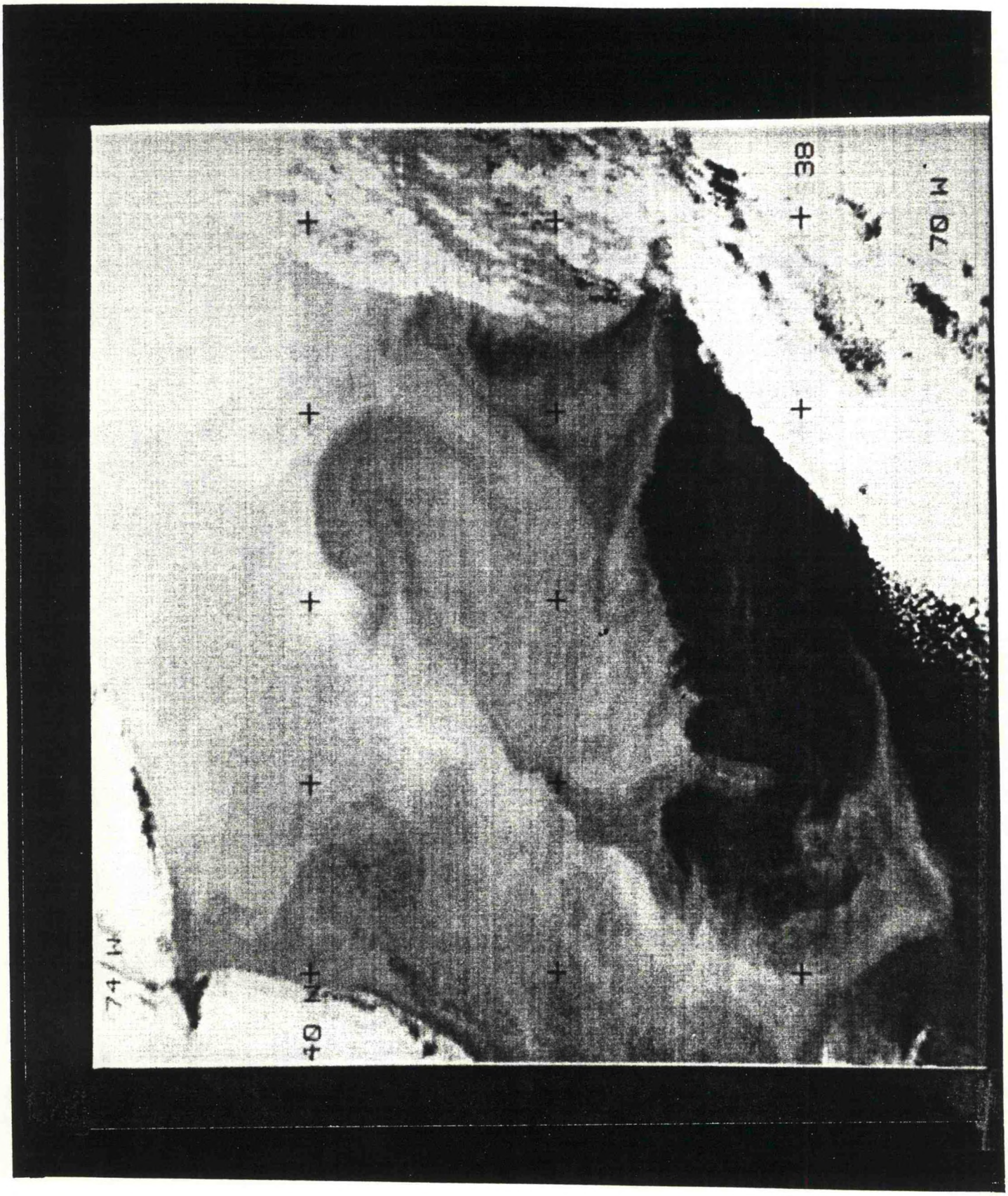

Figure 4. AVHRR satellite image (channel 4) for 24 June 1991 at 0733 UTC.

Figure 5. AVHRR satellite image (channel 4) for 24 June 1991 at 1859 UTC.

Figure 6. AVHRR satellite image (channel 4) for 25 June 1991 at 1847 UTC.

4. RESULTS

In this section we present the feature tracking results for the Slope Water region. First, we examine the problem of earth location error since the accuracy of our feature tracking results depends critically on this aspect of the analysis. Our results include not only the feature tracking displacements and velocities, but also streamline and isotach analyses for the surface flow fields. A brief analysis of the influence of the local winds on the surface flow field follows. Finally, we compare our results with a surface current analysis from the Navy's Fleet Numerical Oceanography Center (FNOC) plus a surface drifter trajectory.

a. Earth location errors

Errors in earth location are related to the particular earth location procedures employed at each facility and most likely will differ between facilities. As a result, we have investigated the magnitude of the earth location errors by comparing known landmarks along the coast with the earth locations which accompany the satellite data provided by NESDIS. Four well-separated locations were chosen for comparison; Great Bay along the coast of southern New Jersey, the Sandy Hook peninsula off northern New Jersey, Fire Island off the southern coast of Long Island (New York) and Mastic Beach, Long Island. Comparisons were made for two descending and three ascending passes acquired near the time of the study. The results are presented in Table 1. The actual and image-derived

locations are given to the nearest hundredth of a degree ($0.01^{\circ} \approx$ 1.1km $\approx$ 1 pixel). These results indicate that the errors are about 1-5 km in latitude and 7-10 km in longitude. These errors, although larger than expected, do not appear to be location dependent. However, the errors are significantly different for ascending and descending orbits. Thus, we have simply averaged these corrections separately for ascending and descending passes and applied them to our feature tracking results.

b. Surface flow fields

To calculate velocity vectors using the feature tracking approach, selected feature displacements (i.e., displacement vectors) were first calculated. To determine the displacements, the locations of selected features in each of the three images were accessed using the SSIPS software.[4] Appropriate earth location error corrections, as described above, were then applied to the first two images which were approximately 12 hours apart. In this case, ascending and descending passes were used, and earth location error corrections were required. For the second pair of images (i.e., the second and third images), no earth location error corrections were needed since both passes were ascending. A third pair of images was also used, consisting of the first and third images; again, earth location error corrections were required. Once the feature locations were determined for each pair of images, the great circle distances between the locations were calculated.

---

[4]SSIPS = Satellite Sea Surface Temperature Image Processing System.

Table 1

Satellite/Image Locations for determining earth location errors

Image Number	Satellite Direction	Sandy Hook	Great Bay	Fire Island	Mastic Beach
1	DSC[1]	40.50[3], 74.09[4]	39.54, 74.42	40.69, 73.34	N/A
2	ASC[2]	40.51, 73.93	39.53, 74.26	N/A	N/A
3	DSC	40.50, 74.08	39.54, 74.42	40.67, 73.29	40.77, 72.96
4	ASC	40.52, 73.91	39.54, 74.25	40.70, 73.16	N/A
5	ASC	40.52, 73.92	39.55, 74.26	40.69, 73.17	40.78, 72.81
Actual Locations:		40.47, 74.01	39.51, 74.33	40.65, 73.25	40.74, 72.88

Errors[5]

1		0.03, 0.08	0.03, 0.09	0.04, 0.09	N/A
2		0.04, -0.08	0.02, -0.07	N/A	N/A
3		0.03, 0.07	0.03, 0.09	0.02, 0.04	0.03, 0.08
4		0.05, -0.10	0.03, -0.08	0.05, -0.09	N/A
5		0.05, -0.09	0.04, -0.07	0.04, -0.08	0.04, -0.07

[1]Descending orbit
[2]Ascending orbit
[3]Latitude
[4]Longitude
[5]To the nearest hundredth of a degree

These distances were then divided by the time intervals between the images to obtain the corresponding velocities.

Twenty-nine displacement and velocity vectors were calculated for each of the two adjacent periods (12 hour interval followed by 24 hour interval) and the entire 36 hour period. The results are tabulated in Tables 2a, 2b and 3. The times shown in Figs. 7-12 correspond to the approximate mid-points of each time period, i.e., 1200 UTC 24 June, 0600 UTC 25 June and 00 UTC 25 June, 1991. The displacement vectors are shown in Figs. 7 and 9 and the velocity vectors in Figs. 8 and 10, for the three feature tracking intervals. The displacements ranged from about 4 to 40 km and the corresponding velocities from about 5 to 40 cm/sec. Since some of the feature tracking results were obtained inshore of the continental shelf margin (i.e., for depths of less than 120m), velocities in this area may also contain tidal influence. Contrary to our expectations, the velocities were not generally continuous for the two adjacent time periods. In many cases, there is significant veering or turning to the right (i.e., anticyclonic rotation; Fig. 8) during the time interval employed. This tendency is not detectable in the surface velocity field determined over a time interval of 36 hours (Fig. 10). The dramatic changes in the direction of flow (Fig. 8) may have been due to inertial oscillations in the surface mixed layer which resulted from a brief, but intense, wind event on 23 June 1991, a day prior to the satellite sequence.

The velocity fields in Figs. 7, 8 and 10 have been subjected

Table 2a. Displacement and Velocity Vectors for the Approximate 12 Hour Period Between 0733 UTC and 1859 UTC on 24 June 1991.

Vector Number	Displacement (km)	Speed (cm/sec)	Direction (°)	Latitude (°)	Longitude (°)
1	8.1	19.8	303.3	40.46	70.48
2	8.9	21.5	239.8	40.32	70.85
3	17.7	42.9	230.8	39.95	71.74
4	3.6	8.8	72.0	39.71	71.47
5	8.4	20.5	246.6	39.66	71.83
6	13.2	32.1	220.5	39.79	71.91
7	19.7	47.8	246.6	39.66	72.10
8	13.1	31.9	211.8	39.24	70.80
9	10.6	25.8	199.0	39.15	72.90
10	13.5	32.8	172.6	39.04	73.32
11	11.3	27.5	207.4	39.01	72.99
12	9.1	22.0	222.4	38.60	73.57
13	9.3	22.6	196.3	38.73	73.32
14	8.0	19.4	213.1	38.48	73.42
15	13.2	32.0	212.1	38.44	72.77
16	9.0	21.8	231.5	38.35	72.50
17	9.9	24.2	206.1	38.46	72.14
18	13.9	33.9	223.9	38.10	72.91
19	14.1	34.2	270.2	38.03	73.37
20	15.6	38.0	179.8	38.00	73.88
21	16.8	40.9	289.4	37.85	73.48
22	13.3	32.2	239.7	37.86	73.13
23	8.4	20.3	237.7	37.75	73.23
24	13.5	32.8	172.7	39.48	71.23
25	4.5	11.0	169.1	39.33	71.75
26	7.0	17.0	80.8	39.38	71.56
27	11.3	27.4	188.8	39.38	71.40
28	14.5	35.3	212.3	39.39	72.71
29	11.3	27.4	217.7	39.33	72.55

Table 2b. Displacement and Velocity Vectors for Approximate 24 Hour Period Between 1859 UTC on 24 June and 1847 UTC on 25 June 1991.

Vector Number	Displacement (km)	Speed (cm/sec)	Direction (°)	Latitude (°)	Longitude (°)
1	13.5	15.7	289.3	40.50	70.60
2	5.2	6.1	257.7	40.29	70.92
3	7.2	8.4	201.0	39.87	71.84
4	11.8	13.8	139.1	39.67	71.40
5	8.9	10.4	331.2	39.68	71.90
6	10.8	12.6	252.0	39.74	72.02
7	11.3	13.2	332.8	39.68	72.23
8	26.1	30.4	236.2	39.13	70.96
9	6.5	7.5	290.2	39.12	72.96
10	5.3	6.2	282.1	38.99	73.34
11	7.5	8.8	207.4	38.93	73.04
12	25.7	30.0	252.3	38.54	73.75
13	18.6	21.7	237.4	38.65	73.42
14	20.0	23.3	247.0	38.41	73.55
15	5.5	6.4	307.4	38.40	72.83
16	11.7	13.7	311.8	38.35	72.59
17	16.0	18.7	299.2	38.46	72.25
18	28.1	32.9	267.7	38.04	73.13
19	22.3	26.1	240.0	37.98	73.56
20	16.4	19.1	245.9	37.90	73.96
21	14.1	16.5	265.5	37.86	73.65
22	24.2	28.3	280.6	37.85	73.33
23	17.3	20.2	234.6	37.68	73.35
24	24.9	29.0	36.1	39.51	71.13
25	7.0	8.2	80.8	39.32	71.71
26	9.0	10.5	60.1	39.40	71.47
27	7.7	9.0	64.1	39.35	71.37
28	3.8	4.4	152.7	39.32	72.74
29	10.3	12.0	229.3	39.26	72.63

Table 3. Displacement and Velocity Vectors for 36 Hour Period Between 0733 UTC on 24 June and 1847 UTC on 25 June 1991.

Vector Number	Displacement (km)	Speed (cm/sec)	Direction (°)	Latitude (°)	Longitude (°)
1	21.5	16.9	294.6	40.48	70.55
2	13.9	11.0	246.4	40.31	70.88
3	24.2	19.0	222.3	39.92	71.76
4	13.6	10.7	125.0	39.66	71.43
5	12.8	10.1	290.4	39.70	71.86
6	23.1	18.2	234.6	39.78	71.97
7	23.3	18.4	275.5	39.71	72.13
8	38.4	30.3	228.0	39.17	70.92
9	12.3	9.7	230.6	39.16	72.93
10	12.8	10.1	195.8	39.04	73.35
11	18.9	14.9	207.4	38.97	73.01
12	33.8	26.7	244.6	38.57	73.71
13	26.4	20.8	224.0	38.68	73.40
14	27.0	21.3	237.5	38.44	73.53
15	13.8	10.9	235.5	38.46	72.79
16	15.9	12.5	278.1	38.38	72.55
17	18.4	14.5	266.5	38.49	72.22
18	39.4	31.1	253.5	38.09	73.07
19	35.2	27.8	251.5	37.98	73.48
20	26.9	21.2	213.8	37.97	73.96
21	30.3	23.9	278.5	37.84	73.56
22	35.3	27.8	266.4	37.88	73.27
23	25.7	20.2	235.6	37.71	73.31
24	17.7	13.9	67.7	39.57	71.15
25	8.5	6.7	113.3	39.34	71.71
26	15.7	12.4	69.2	39.39	71.51
27	9.4	7.4	146.5	39.39	71.36
28	16.8	13.2	201.1	39.38	72.69
29	21.4	16.9	223.2	39.30	72.59

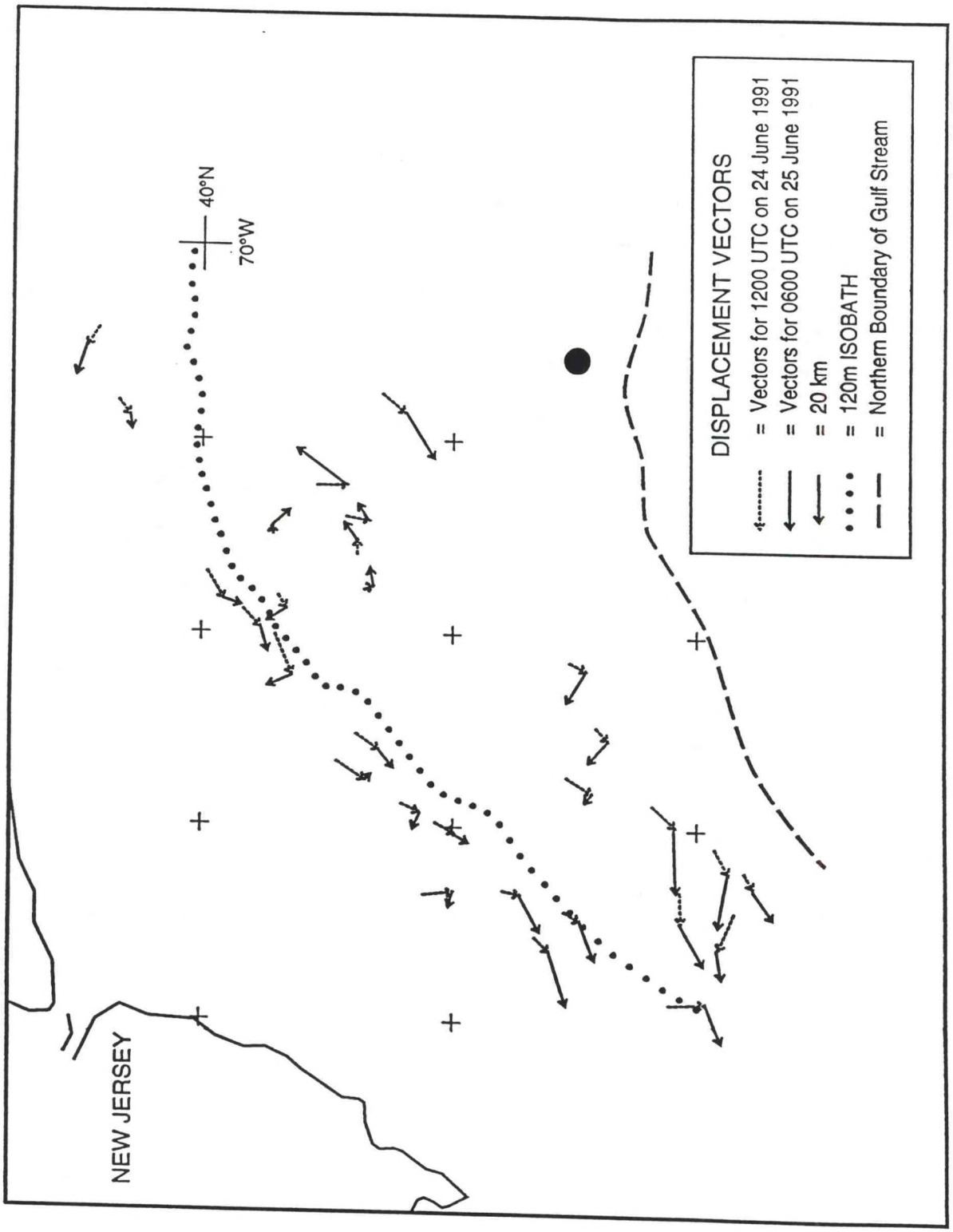

Figure 7. Surface displacement vectors derived from AVHRR satellite images from 24 June at 0733 UTC to 24 June at 1859 UTC and from 24 June at 1859 UTC to 25 June at 1847 UTC. The black circle at 38.5°N, 70.6°W represents the location of NDBC buoy number 44004.

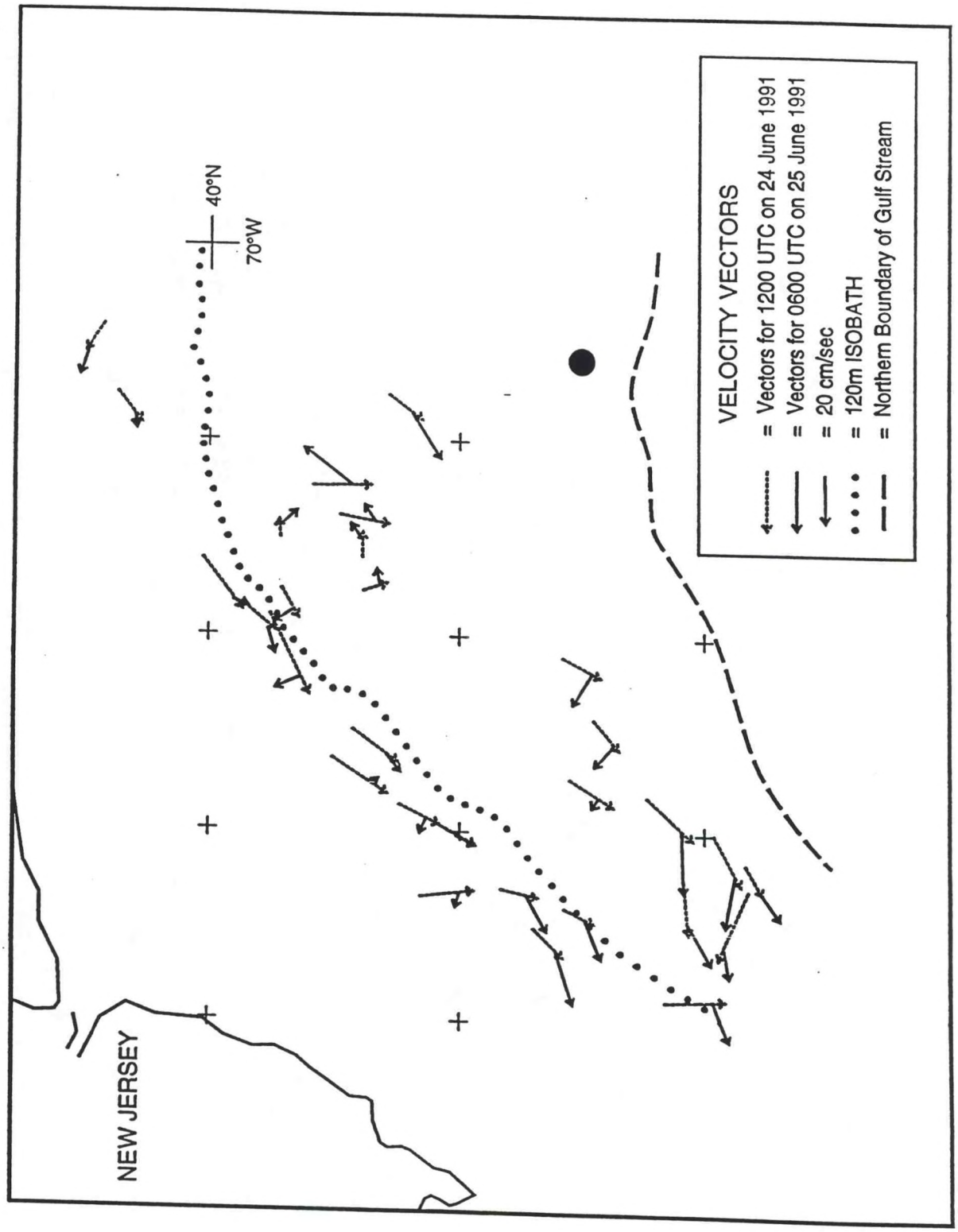

Figure 8. Surface velocity vectors based on the displacement vectors from Fig. 6, for time intervals between images of 11.43 hours (dashed arrows) and 23.80 hours (solid arrows).

FIG A

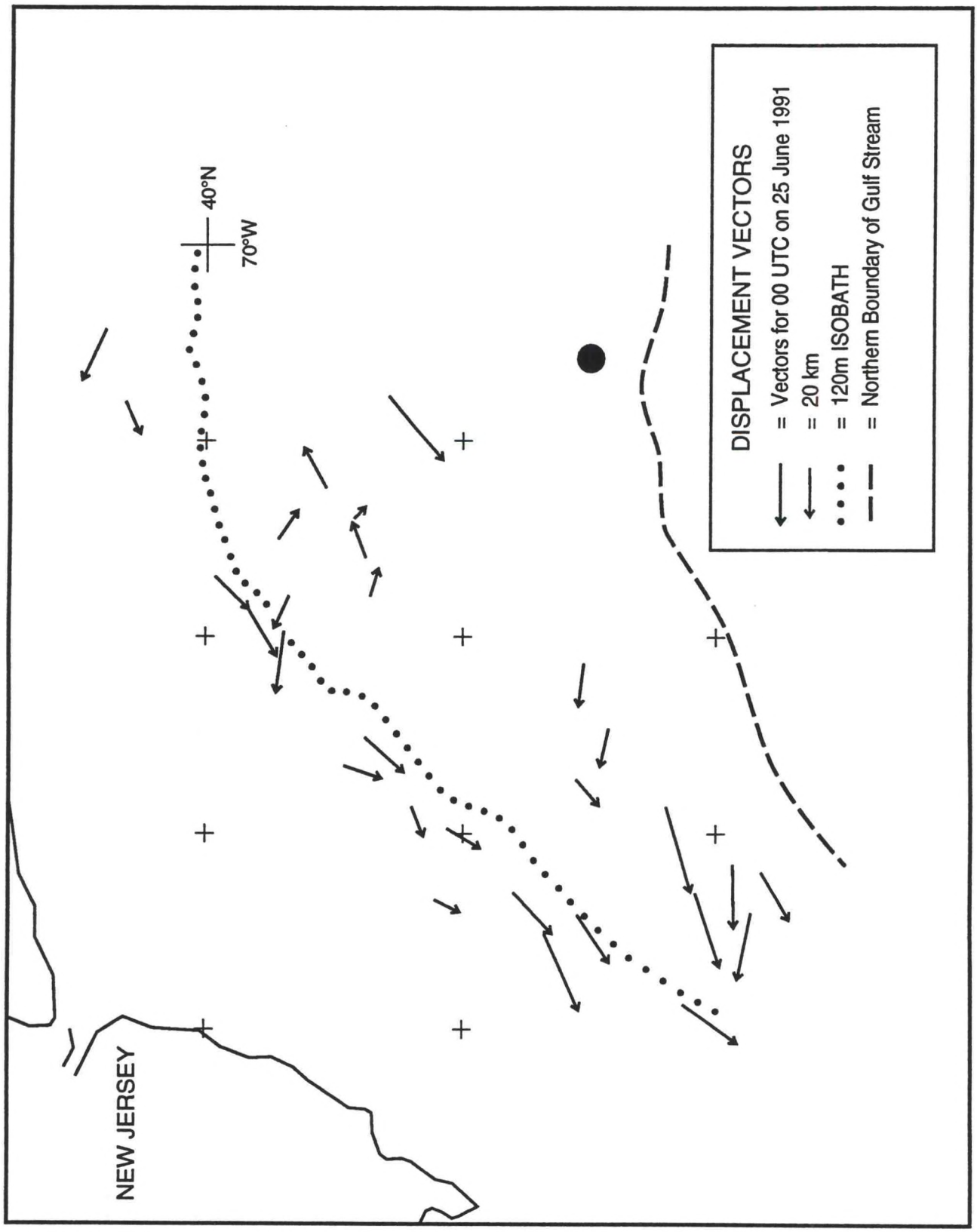

Figure 9. Displacement vectors for the 36 hour period between the first and third images, centered approximately at 00 UTC, 25 June 1991.

FIG B

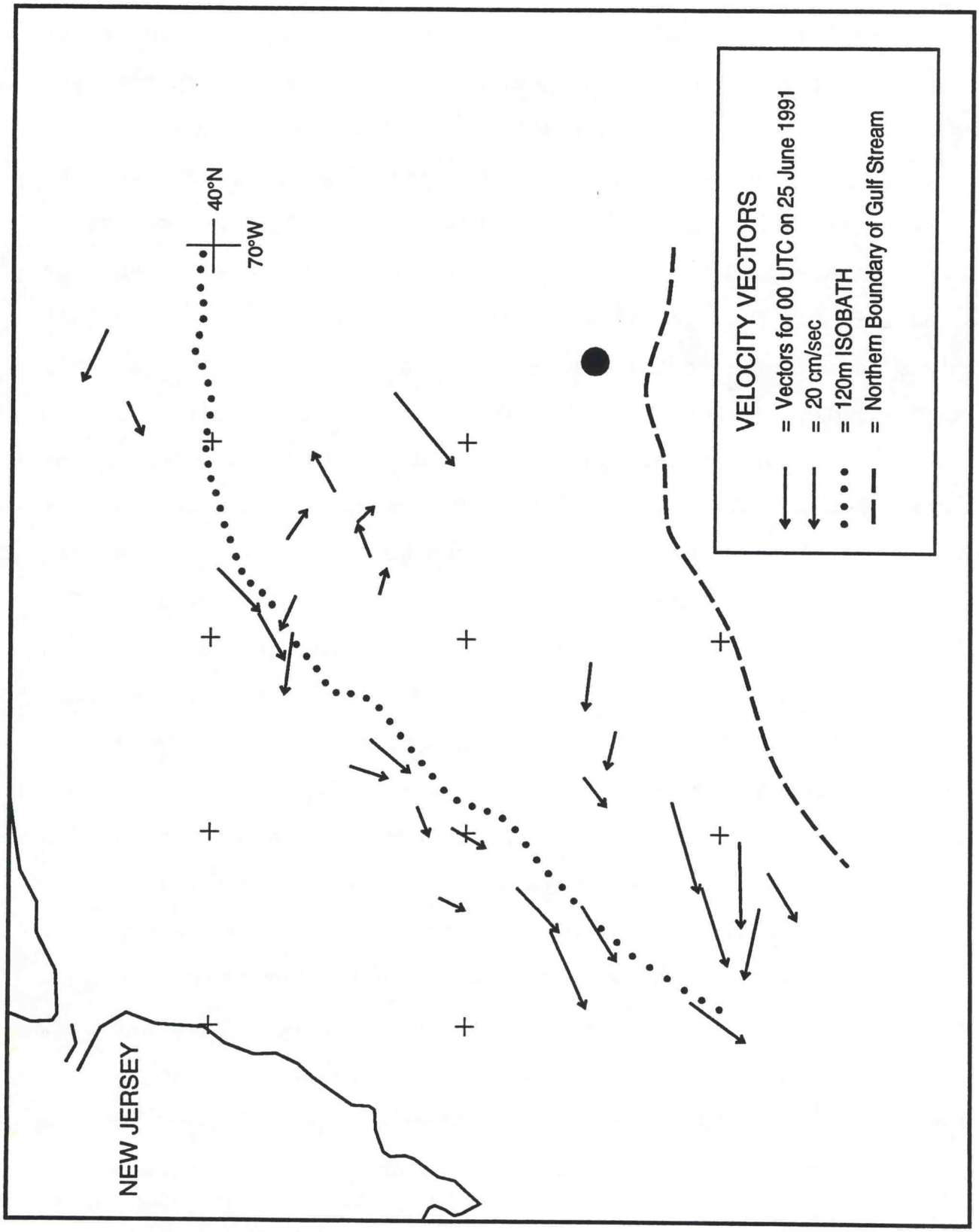

Figure 10. Velocity vectors for the 36 hour period between the first and third images, centered approximately at 00 UTC, 25 June, 1991.

to streamline and isotach analysis. Streamlines for the 12 and 24 hour analysis intervals are shown in Fig. 11 and are taken to be centered at 1200 UTC 24 June and 0600 UTC 25 June, respectively. For the first period (i.e., the 12 hour interval), the direction of flow is clearly to the SW. For the second period, however, the flow is wave-like, with a major change in flow direction occurring around the eddy located at 39.5°N, 71.5°W. A major wind event on June 23rd may have generated inertial oscillations in the surface mixed layer which contributed to this wave-like behavior (as well as the semidiurnal tide). The pattern of flow associated with the eddy located at 39.5°N, 71.5°W is complicated, but appears to be anticyclonic. Although this eddy appears to have originated from the shelf/slope front, its history can be traced back to the Gulf Stream where it originally developed from a meander (Aikman, 1991). Although two anticyclonic centers in close proximity are depicted for the second period, it is likely that there is only one center, as shown for the first period. Two cyclonic centers further to the SW are depicted in the second analysis as well (plus one cyclonic center during the first period). However, there are no in situ data available to confirm the existence of these features.

Isotach analyses for both intervals are shown in Fig. 12. Higher speeds for both periods tend to be located near 39°N, 71°W and to the SW near 38°N, 73.3°W. There is a wave-like pattern, similar to the wave-like perturbation in the streamlines for the isotach contours for the second period, again reflecting the possible influence of inertial oscillations. Finally, streamlines

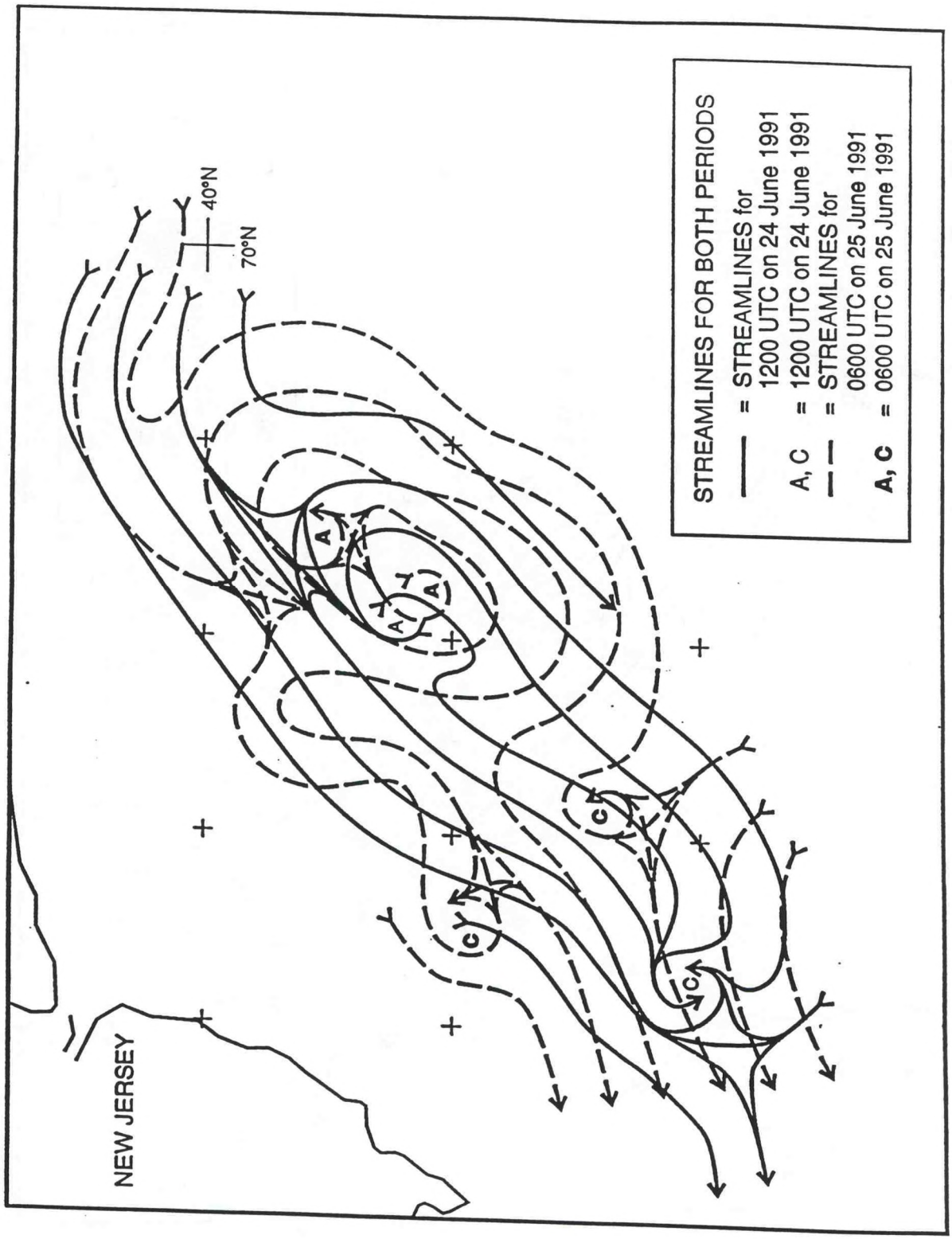

Figure 11. Streamline analyses for both periods, the first between 0733 UTC and 1859 UTC on 24 June, and the second between 1859 UTC on 24 June and 1847 UTC 25 June, 1991.

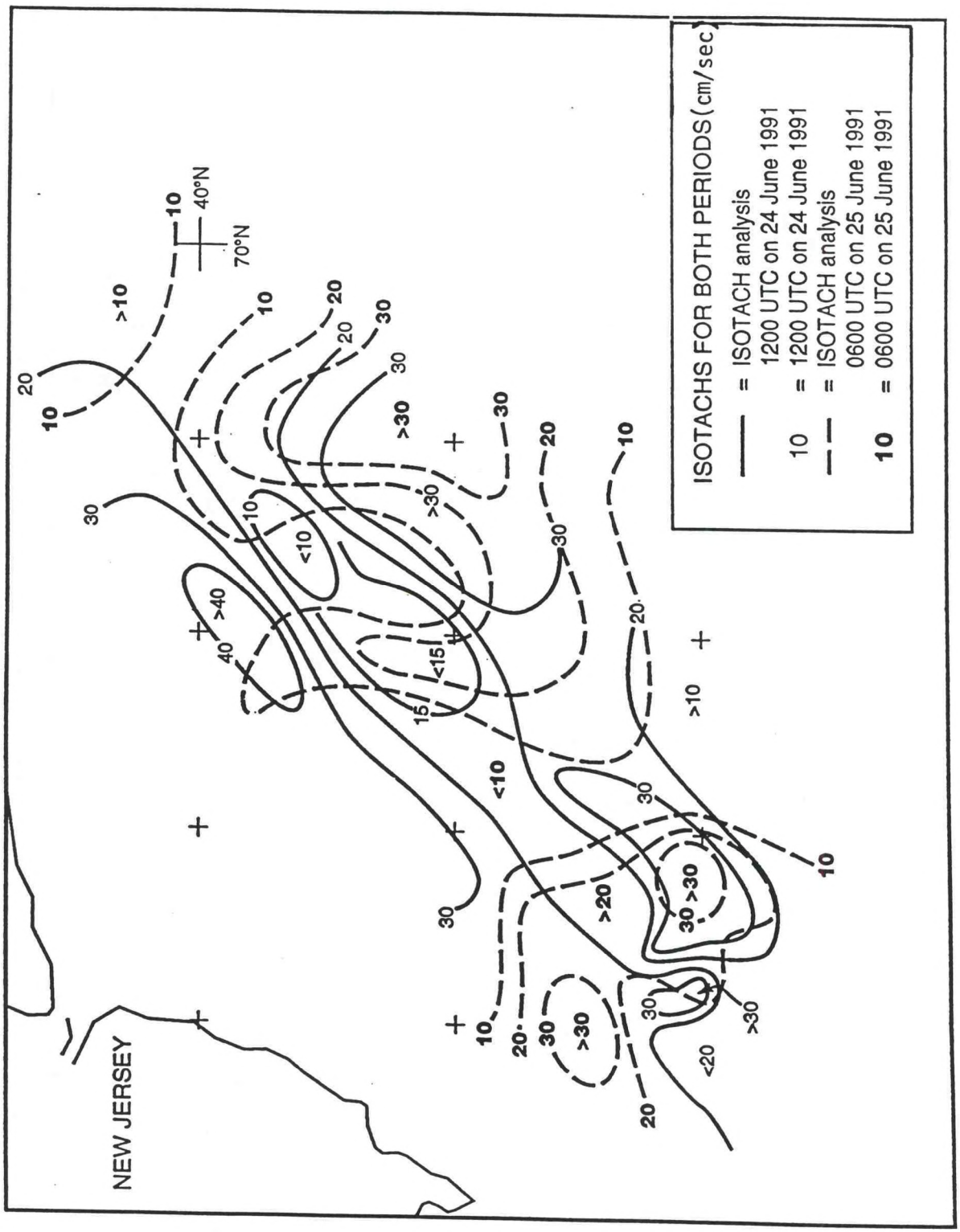

Figure 12. Isotach analyses for both periods (as in Figure 11).

and isotachs for the velocity vectors obtained for the entire 36 hour period are shown in Fig. 13, and reveal patterns of flow and speed which tend to obscure the wave-like oscillation that occurred during the second analysis interval.

c. Wind-driven contribution

We used a modified form of Ekman's theory for pure wind drift to estimate the contribution of the surface wind to the surface currents in the Slope Water region (Madsen, 1977). Unlike Ekman who assumed a constant vertical eddy viscosity, Madsen adopted a vertical eddy viscosity which increased linearly with depth from a value of zero at the free surface. His steady-state solution produced surface drift currents which deviated from the direction of the surface wind by roughly 10°, a value much smaller than that obtained by Ekman (45°), and much closer to observations.

Surface winds were obtained from NMC's Aviation Forecast Model. These winds are available on a 1° x 1° grid, globally. The lowest sigma layer winds from the model were reduced to a height of 10m using standard log profile scaling (which assumes a neutrally stable boundary layer). These winds, available at synoptic times, were interpolated in time to the mid-points of the feature tracking periods. These values were then interpolated spatially to produce winds at the various surface flow vector locations. Following Madsen's approach, the vertical eddy viscosity increased linearly with depth. The model-derived winds produced surface currents whose directions varied between 8 and 15° to the right of the surface wind (i.e., northern hemisphere) and whose speeds were 2-3%

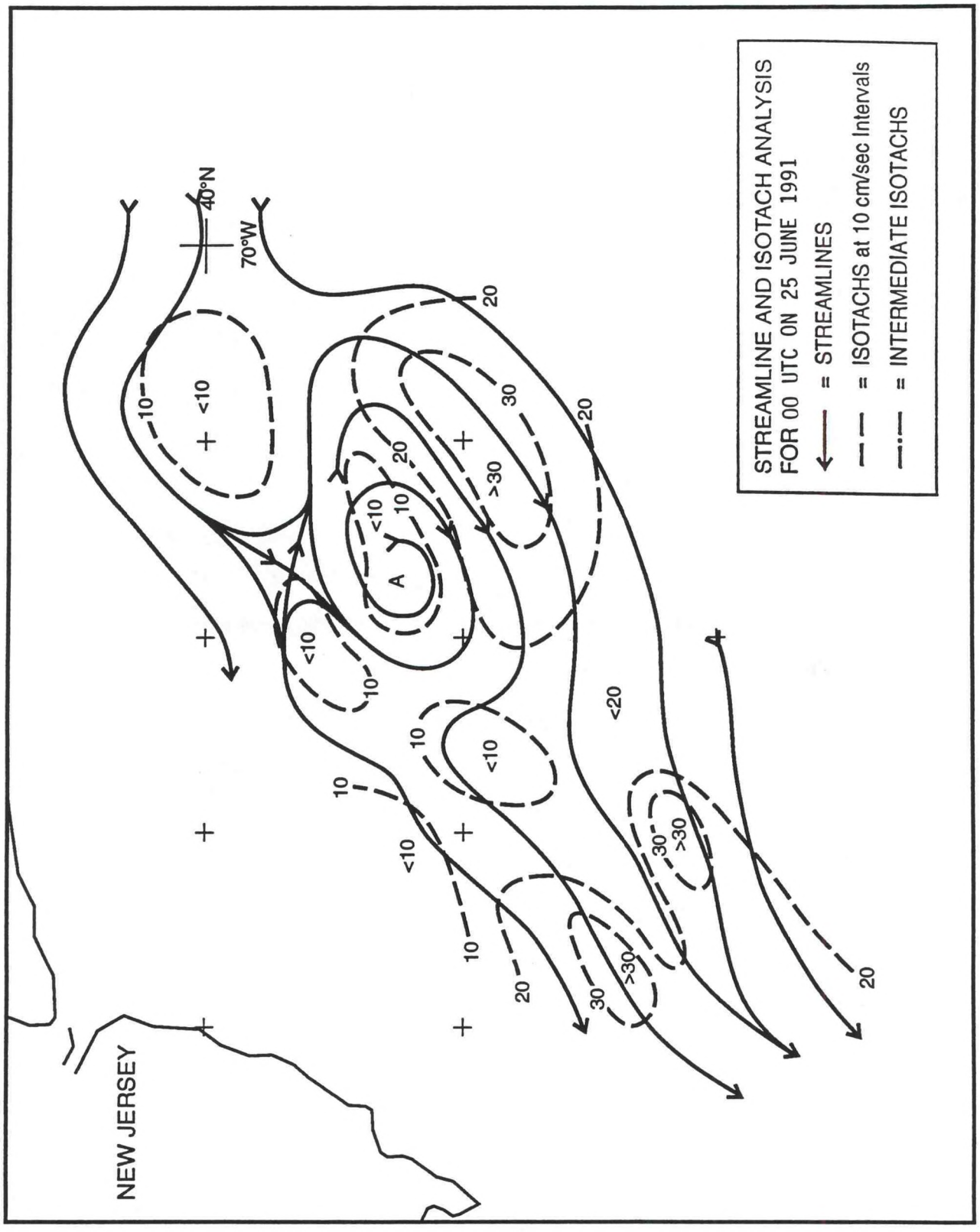

Figure 13. Streamline and isotach analyses for the 36 hour velocity vectors centered on 00 UTC, 25 June 1991.

of the wind speed. The results for the second time period are shown in Fig. 14. The maximum wind-driven contribution is about 18 cm/sec, a value considerably smaller than the velocities obtained by feature tracking in the same area (~30 cm/sec). The primary wind direction is from the NE, contrary to the climatological winds which are typically from the SW for this time of year (Meserve, 1974). This contribution from the wind is generally in the direction of the satellite-derived surface flow and thus contributes constructively to the overall flow in this area. In most cases, the wind-driven component was less than half of the observed velocity, indicating the importance of other processes which also contribute to the surface flow in this area. It is important to recognize that the ocean's response to wind forcing is multifaceted and that in addition to a steady-state Ekman-type response, transient responses which may include the generation of inertial oscillations is likely, if the wind field was changing rapidly, as it was in our case. Also, the influence of remote forcing by the wind may be significant. Thus, the ocean's overall response to the variable wind conditions encountered is undoubtedly far more complex than can be accounted for by considering only a steady-state (Ekman-like) contribution.

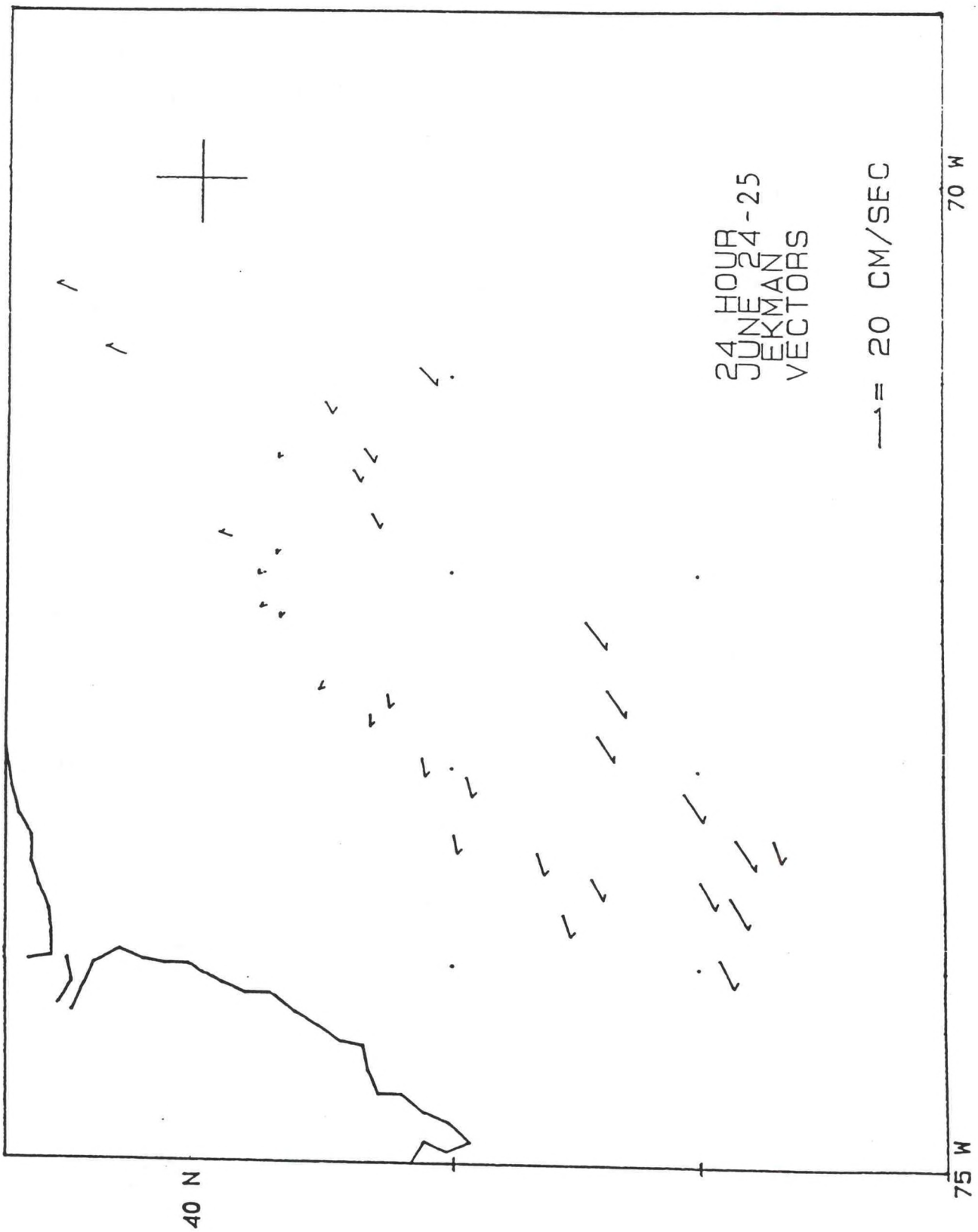

Figure 14. Surface velocity vectors due to wind-driven Ekman transport (based on Madsen, 1977).

d. Comparisons with other analyses

First, we compare our results with a surface current analysis produced by Fleet Numerical Oceanography Center (FNOC) based on the Navy's Thermal Ocean Prediction System (TOPS) model (Clancy et al., 1990) and surface winds obtained from other sources. Geostrophic velocities are derived from the TOPS model, and a wind-driven Ekman component is calculated from the surface winds. The geostrophic and Ekman components are then combined to produce the surface flow field on a high-resolution (~20km) grid. The FNOC surface current field for 24 June 1991 is shown in Fig. 15. A comparison of the FNOC field with our surface flow fields indicates that in most cases, the direction of flow is generally more to the west in the FNOC field whereas our results indicate flow more to the SW. Also, our directions and speeds show much greater variability than that indicated in the relatively smooth FNOC field. More favorably, the FNOC field indicates an anticyclonic eddy at the same location where we have indicated eddy-like circulation.

A Lagrangian trajectory from a satellite-tracked drifting buoy is shown in Fig. 16 which overlaps the period of our study.[5] The nearest surface velocity vectors from our analysis (Fig. 8) have been overplotted for comparison. Although the satellite-derived flow vectors located over the northern half of the trajectory were acquired 3-5 weeks after the trajectory data, the directions of flow appear to be in close qualitative agreement (speeds were not compared).

---

[5]This figure was kindly provided to us by Dr. Frank Aikman of NOS.

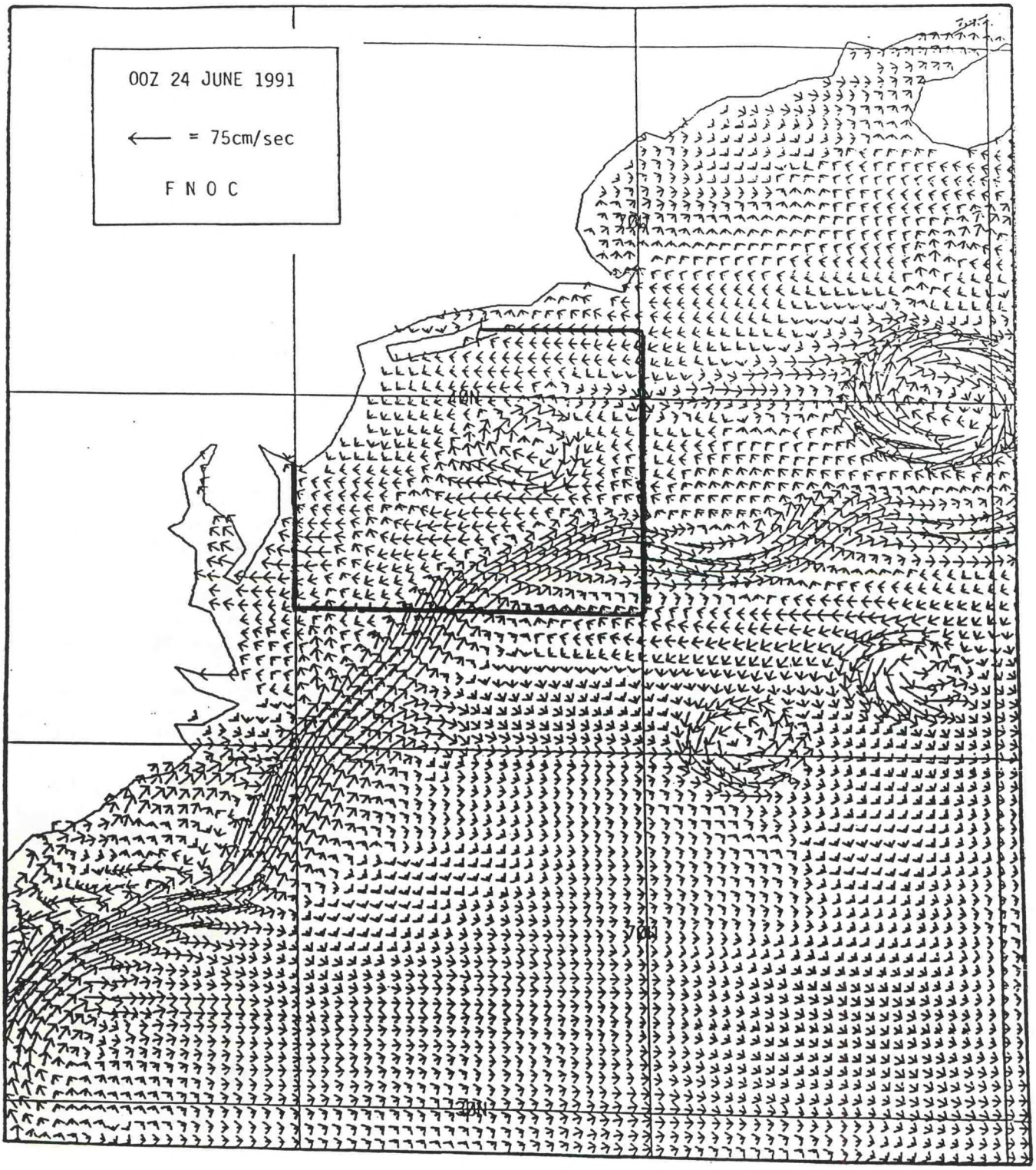

Figure 15. Surface current analysis from FNOC for 24 June 1991 at 0000 UTC (see text for details).

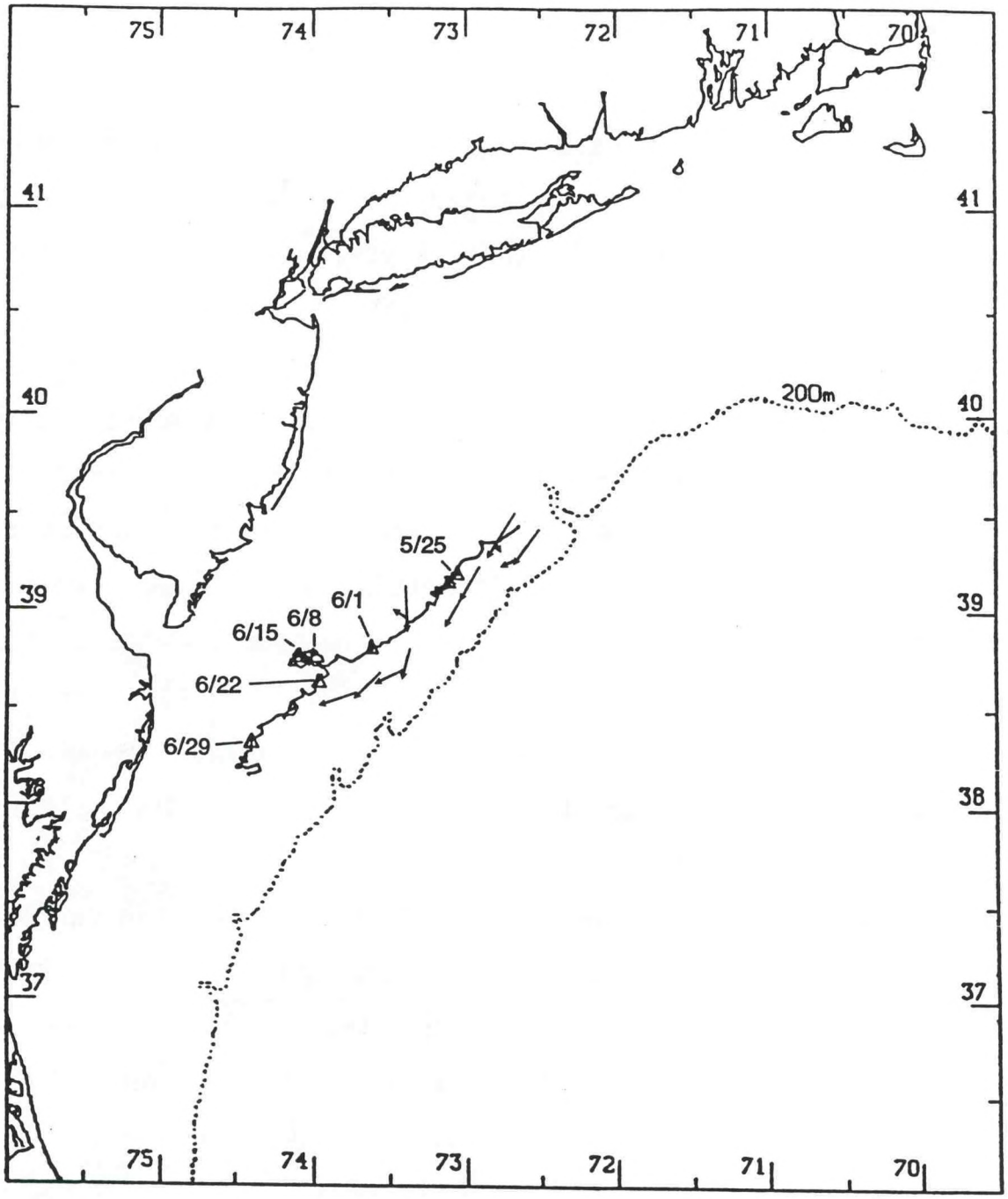

Figure 16. Satellite-tracked drifting buoy trajectory from 5/18/91 to 6/31/91 (Aikman, 1991). Nearest surface flow vectors from Figure 8 have been included for comparison (24-25 June 1991).

5. DISCUSSION

The motion of individual rings includes both the velocity of the rings relative to the Slope Water plus the velocity of the Slope Water itself. Cornillon et al.(1989) explicitly separate these motions using the method of satellite feature tracking to estimate the surface motion of the Slope Water; thus, we can compare our results directly with those of Cornillon et al. They obtained surface velocities west of the New England Seamount Chain of 8-20 cm/sec at a direction of 226°. For comparison, we obtain speeds of 10-31 cm/sec and a median direction of 236°, based on the 36 hour velocity vectors, excluding those surface flow estimates associated with the eddy located at 39.5°N, 71.5°W. Although the agreement in direction is close, the somewhat higher speeds we obtain may be due in part to the inclusion of surface flow estimates associated with the warm intrusion at 38.3°N, 73.2°W originating in the Gulf Stream plus the fact that the wind forcing was constructive with repsect to the prevailing surface flow direction (an unusual occurrence for this time of year). Also, the observations of Cornillon et al. were generally located further east (~68-72°W) than our own (~70-74°W). Finally, the inclusion of wave-like motions in the surface velocity field has also contributed to our estimates for the particular time period during which the satellite data were acquired.

Just prior to, and during, the period of satellite observations, a major wind event occurred (Fig. 17). Peak winds of

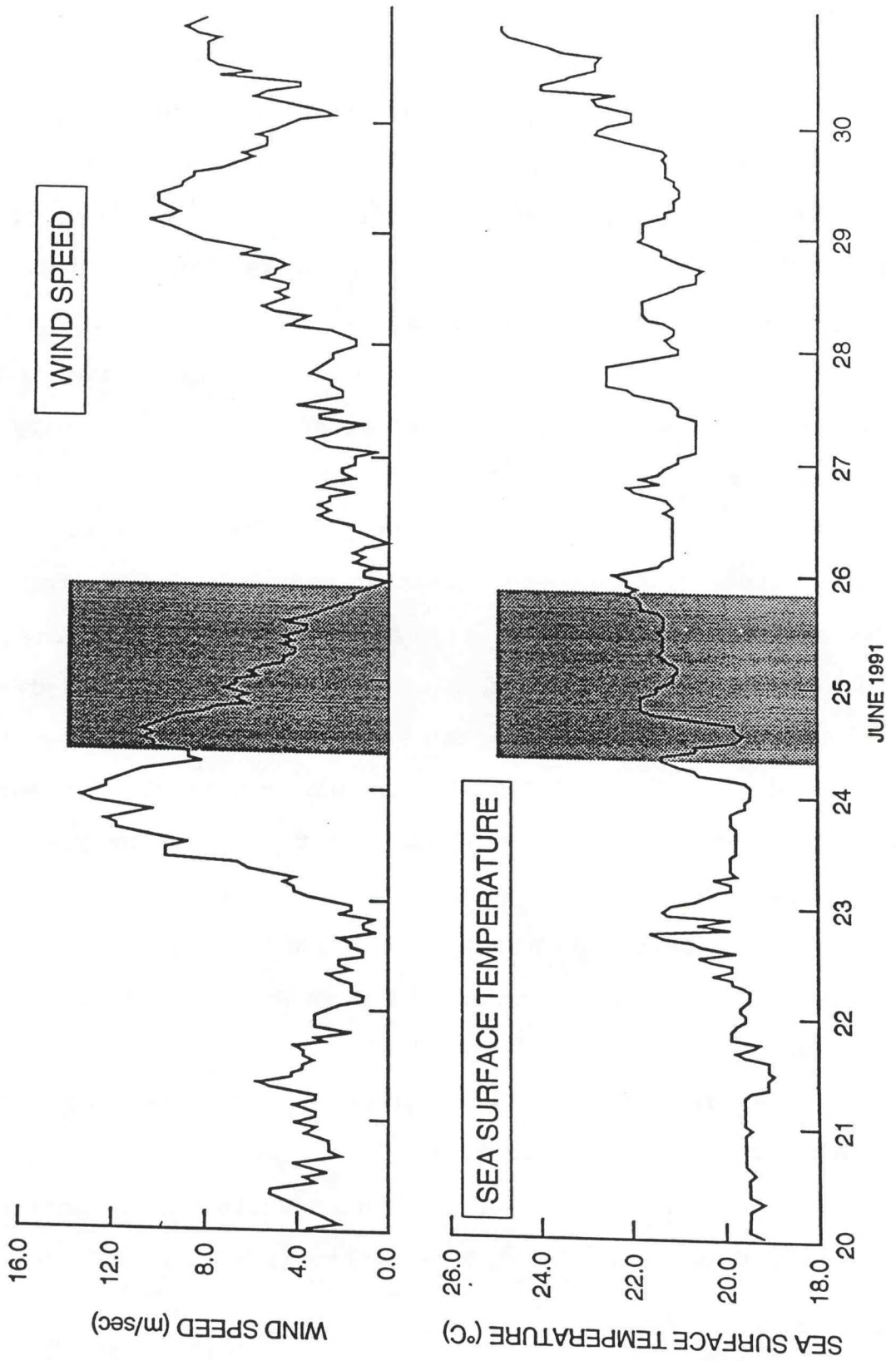

Figure 17. Wind speed and sea surface temperature time series from NDBC buoy number 44004 (38.5°N, 70.6°W). Shaded area corresponds to period when AVHRR satellite imagery was acquired.

14 m/sec occurred on 23 June, based on wind data acquired at the National Data Buoy Center (NDBC) environmental data buoy located at 38.5°N, 70.6°W. As the winds subsided, oscillations in SST beginning on 24 June occurred with periods ranging from about 12 to 24 hours. The inertial period at 39°N is 19 hours; thus, it is possible that these variations in SST represent inertial oscillations of the surface mixed layer resulting from the wind impulse on 23 June. Wind impulses of sufficient intensity whose durations are short relative to the local inertial period often produce such transient behavior (e.g., Webster, 1968; Pollard, 1970). Consequently, the dramatic changes in surface flow (direction in particular) during the second feature tracking period may have been due to a brief wind event which produced inertial oscillations in the surface mixed layer. According to the theoretical results of Pollard (1970), the maximum inertial velocities that result from impulsive wind forcing tend to occur two to four inertial periods after the wind stress has been applied. Thus, a delay of approximately 30 hours in our case between the occurrences of the wind event and the oscillations in SST are not seriously at odds with the results of Pollard.

The sampling employed in this study (~12, ~24 and ~36 hour intervals) brings into question the assumption of rectilinear motion between satellite samples[6]. Our results were significantly different for each of the sample intervals employed. The clear

---

[6]Clearly, when only two satellite samples are available and with no additional information, there is no alternative to the assumption of rectilinear motion.

implication from the results presented here is that relatively short sample intervals (12 hours or less) are required, in order to accept the assumption of rectilinear motion. To achieve even shorter intervals between samples for AVHRR data, imagery from two satellites will be required. Coverage from two satellites could provide imagery at roughly six-hour intervals. However, as the intervals between images becomes shorter, the corresponding displacements may become so small that earth location and co-registration errors become a limiting factor. For example, for a velocity of 10 cm/sec, the corresponding displacement over a six-hour period would only be 2.2 km, or about 2 pixels for full-resolution AVHRR data. Clearly, a problem arises for sampling intervals as short as six hours unless the speeds in the domain of interest are sufficiently high.

6. CONCLUSIONS

Although the method of satellite feature tracking for estimating surface currents has not been applied extensively to the Slope Water region considered here (37-41°N, 70-74°W), the results of this study do indicate that reasonable values for surface velocity (speed and direction) were obtained. These results generally compare favorably with other oceanographic analyses for this region.

Streamline and isotach analyses of the satellite-derived surface flow vectors extended the utility of the individual observations, and thus our ability to interpret the results.

Just prior to the period of observation, a major wind event may have generated inertial oscillations in the surface mixed layer which produced a major wave-like perturbation in the surface flow field. This wave-like behavior was revealed in both the streamline and the isotach analyses. The occurrence of this transient behavior emphasizes the importance of utilizing relatively short intervals between satellite images to justify the assumption of rectilinear motion. Intervals of approximately 12 hours may provide acceptable sampling for satellite coverage that (1) satisfies the assumption of rectilinear motion between samples, and (2), avoids problems associated with errors in earth location and co-registration.

The results of this study provide a starting point for developing operational procedures to estimate time dependent

surface currents in coastal areas. Consequently, these results should be of interest to NOAA's Coastal Ocean Program where the need for real-time ocean surface currents in selected COASTWATCH areas has been identified.

7. ACKNOWLEDGEMENTS

The authors would like to thank Joanne Nault, Paul Long, Susan Hubbard and Frank Aikman for various contributions during the course of this study. Also, the encouragement provided by D. B. Rao and his thorough review of this report are appreciated. Finally, we acknowledge NOAA's Coastal Ocean Program for providing the impetus to initiate and complete this study.

8. REFERENCES

Abbott, M. R. and D. B. Chelton, 1991: Advances in passive remote sensing of the ocean. U.S. National Report 1987-1990, Contributions in Oceanography, American Geophysical Union, 571-589.

Aikman, F., 1991: Personal communication.

Beardsley, R. C. and C. N. Flagg, 1975: The water structure, mean currents, and shelf-water/slope water front of the New England continental shelf. Seventh Liege Colloquium on Ocean Hydrodynamics, 10, 209-226.

Clancy, R. M., P. A. Phoebus and K. D. Pollak, 1990: An operational global-scale ocean thermal analysis system. J. Atmos. and Oceanic Tech., 7, 233-254.

Cornillon, P. C., R. Weyer and G. Flierl, 1989: Translational velocity of warm-core rings relative to the Slope Water. J. Phys. Oceanogr., 19, 1317-1332.

Crosby, D. S., L. C. Breaker and W. H. Gemmill, 1991: A proposed definition for vector correlation in geophysics: theory and application. Submitted to the Journal of Atmospheric and Oceanic Technology.

Emery, W. J., A. C. Thomas, M. J. Collins, W. R. Crawford and D. L. Mackas, 1986: An objective method for computing advective surface velocities from sequential infrared satellite images. J. Geophys. Res., 91, 12,865-12,878.

Kamachi, M., 1989: Advective surface velocities derived from sequential images for rotational flow field: limitations and applications of maximum cross-correlation method with rotational registration. J. Geophys. Res., 94, 18227-18233.

Kouzai, K. and K. Tsuchiya, 1990: Estimation of surface current velocities of the Kuroshio using single NOAA AVHRR image. J. Remote Sensing Society of Japan, 10, 13-23.

Leese, J. A., C. S. Novak and B. B. Clarke, 1971: An automated technique for obtaining cloud motion from geosynchronous satellite data using cross correlation. J. Appl. Meteor., 10, 110-132.

Madsen, O. S., 1977: A realistic model of the wind-induced Ekman boundary layer. J. Phys. Ocean., 7, 248-255.

Mamayev, O. I., 1975: Temperature - Salinity Analysis of World Ocean Waters. Elsevier Oceanography Series, 11, Elsevier, Amsterdam.

Meserve, J. M., 1974: U.S. Navy Marine Climate Atlas of the World, Vol. 1 - North Atlantic Ocean, National Climatic Data Center, U.S. Department of Commerce for the Commander, Naval Weather Service Command. [available from the U.S. Government Printing Office]

Mooers, C. N. K., Flagg, C. N., Boicourt, W. C., 1978: Prograde and retrograde fronts. Oceanic Fronts in Coastal Processes. Ed. M. Bowman, W. Esaias. Springer-Verlag, 43-58.

Ninnis, R. M., W. J. Emery and M. J. Collins, 1986: Automated extraction of pack ice motion from advanced very high resolution radiometer imagery. J. Geophys. Res., 91, 10,725-10,734.

Njoku, E. G., T. P. Barnett, R. M. Laurs and A. C. Vastano, 1985: Advances in satellite sea surface temperature measurements and oceanographic applications. J. Geophys. Res., 90, 11573-11586.

Pollard, R. T., 1970: On the generation by winds of inertial waves in the ocean. Deep Sea Res., 17, 795-812.

Richardson, P. L., 1983: Gulf Stream Rings. In Eddies in Marine Science, A. R. Robinson (ed), New York. Springer-Verlag, 19-45.

Rosenfeld, A. 1961: Automated detection of changes in reconnaissance data. Fifth Nat. Convention of Milit. Elec. Inst. Radio. Engineers, Budd Electronics, Long Island City.

Sadler, J. C., 1962: Utilization of meteorological satellite cloud data in tropical meteorology. USAF Cambridge Res. Lab., Res. Note AFCRL, 62-829.

Sadler, J. C., 1963: Tiros observations of the summer circulation and weather patterns of the eastern north pacific. Hawaii Inst. Geophys. Rept. No. 40.

Svejkovsky, J., 1988: Sea surface flow estimation from Advanced Very High Resolution Radiometer and Coastal Zone Color Scanner Satellite Imagery: a verification study. J. Geophys. Res., 93, 6735-6743.

Tchernia, P., 1980: Descriptive Regional Oceanography. Pergamon Press, Oxford.

Thompson, E., 1991: Personal communication.

Tokmakian, R., P. T. Strub and J. M. McClean-Padman, 1990: Evaluation of the maximum cross-correlation method of estimating sea surface velocities from sequential satellite imagery. J. Atmos. and Oceanic Tech., 7, 852-865.

Vukovitch, F. M., 1985: Comparison of surface geostrophic currents calculated using satellite data and hydrographic data, final report. Contr. N402730, Fla. Inst. Oceanogr., Miami, Fla.

Wahl, D. D. and J. J. Simpson, 1990: Physical processes affecting the objective determination of near-surface velocity from satellite data. J. Geophys. Res., 95, 13,511-13,528.

Webster, F., 1968: Observations of inertial-period motions in the deep sea. Rev. Geophys., 6, 473-490.

No. 29. Chen, H. S., 1989: Infinite Elements for Combined Diffration and Refraction . Conference Preprint, Seventh International Conference on Finite Element Methods Flow Problems, Huntsville, Alabama, 6pp.

NO. 30. Chao, Y. Y., 1989: An Operational Spectral Wave Forecasting Model for the Gulf of Mexico. Proceedings of 2nd International Workshop on Wave Forecasting and Hindcasting, 240-247.

No. 31. Esteva, D. C., 1989: Improving Global Wave Forecasting Incorporating Altimeter Data. Proceedings of 2nd International Workshop on Wave Hindcasting and Forecasting, Vancouver, B.C., April 25-28, 1989, 378-384.

No. 32. Richardson, W. S., J. M. Nault, D. M. Feit, 1989: Computer-Worded Marine Forecasts. Preprint, 6th Symp. on Coastal Ocean Management Coastal Zone 89, 4075-4084.

No. 33. Chao, Y. Y., T. L. Bertucci, 1989: A Columbia River Entrance Wave Forecasting Program Developed at the Ocean Products Center. Techical Note/NMC Office Note 361.

No. 34. Burroughs, L. D., 1989: Forecasting Open Ocean Fog and Visibility. Preprint, 11th Conference on Probability and Statisitcs, Monterey, Ca., 5pp.

No. 35. Rao, D. B., 1990: Local and Regional Scale Wave Models. Proceeding (CMM/WMO) Technical Conference on Waves, WMO, Marine Meteorological of Related Oceanographic Activities Report No. 12, 125-138.

No. 36. Burroughs, L.D., 1991: Forecast Guidance for Santa Ana conditions. Technical Procedures Bulletin No. 391, 11pp.

No. 37. Burroughs, L. D., 1989: Ocean Products Center Products Review Summary. Technical Note/NMC Office Note No. 359. 29pp.

No. 38. Feit, D. M., 1989: Compendium of Marine Meteorological and Oceanographic Products of the Ocean Products Center (revision 1). NOAA Technical Memo NWS/NMC 68.

No. 39. Esteva, D. C., Y. Y. Chao, 1991: The NOAA Ocean Wave Model Hindcast for LEWEX. Directional Ocean Wave Spectra, Johns Hopkins University Press, 163-166.

No. 40. Sanchez, B. V., D. B. Rao, S. D. Steenrod, 1987: Tidal Estimation in the Atlantic and Indian Oceans, 3° x 3° Solution. NASA Technical Memorandum 87812, 18pp.

No. 41. Crosby, D.S., L.C. Breaker, and W.H. Gemmill, 1990: A Difintion for Vector Correlation and its Application to Marine Surface Winds. Technical Note/NMC Office Note No. 365, 52pp.

No. 42. Feit, D.M., and W.S. Richardson, 1990: Expert System for Quality Control and Marine Forecasting Guidance. Preprint, 3rd Workshop Operational and Metoerological, CMOS, 6pp.

No. 43. Gerald, V.M., 1990: OPC Unified Marine Database Verification System. Technical Note/NMC Office Note No. 368, 14pp.

No. 44. Wohl, G.M., 1990: Sea Ice Edge Forecast Verification System. National Weather Association Digest, (submitted)

No. 45. Feit, D.M., and J.A. Alpert, 1990: An Operational Marine Fog Prediction Model. NMC Office Note No. 371, 18pp.

No. 46. Yu, T. W. , and R. L. Teboulle, 1991: Recent Assimilation and Forecast Experiments at the National Meteorological Center Using SEASAT-A Scatterometer Winds. Technical Note/NMC Office Note No. 383, 45pp.

No. 47. Chao, Y.Y., 1990: On the Specification of Wind Speed Near the Sea Surface. Marine Forecaster Training Manual, (submitted)

No. 48. Breaker, L.C., L.D. Burroughs, T.B. Stanley, and W.B. Campbell, 1992: Estimating Surface Currents in the Slope Water Region Between 37 and 41°N Using Satellite Feature Tracking. Technical Note, 47pp.

No. 49. Chao, Y.Y., 1990: The Gulf of Mexico Spectral Wave Forecast Model and Products. Technical Procedures Bulletin No. 381, 3pp.

No. 50. Chen, H.S., 1990: Wave Calculation Using WAM Model and NMC Wind. Preprint, 8th ASCE Engineering Mechanical Conference, 1, 368-372.

No. 51. Chao, Y.Y., 1990: On the Transformation of Wave Spectra by Current and Bathymetry. Preprint, 8th ASCE Engineering Mechnical Conference, 1, 333-337.

No. 52. Breaker, L.C., W.H. Gemmill, and D.S. Crosby, 1990: A Vector Correlation Coefficient in Geophysical: Theoretical Background and Application. Deep Sea Research, (to be submitted)

No. 53. Rao, D.B., 1991: Dynamical and Statistical Prediction of Marine Guidance Products. Proceedings, IEEE Conference Oceans 91, 3, 1177-1180.

No. 54. Gemmill, W.H., 1991: High-Resolution Regional Ocean Surface Wind Fields. Proceedings, AMS 9th Conference on Numerical Weather Prediction, Denver, CO, Oct. 14-18, 1991, 190-191.

No. 55. Yu, T.W., and D. Deaven, 1991: Use of SSM/I Wind Speed Data in NMC's GDAS. Proceedings, AMS 9th Conference on Numerical Weather Prediction, Denver, CO, Oct. 14-18, 1991, 416-417.

No. 56. Burroughs, L.D., and J.A. Alpert, 1992: Numerical Fog and Visiability Guidance in Coastal Regions. Technical Procedures Bulletin. (to be submitted)

No. 57. Chen, H.S., 1992: Taylor-Gelerkin Method for Wind Wave Propagation. ASCE 9th Conf. Eng. Mech. (in press)